nature genetics

BAZ2A (TIP5) is involved in epigenetic alterations in prostate cancer and its overexpression predicts disease recurrence

Lei Gu[1,2,16,17], Sandra C Frommel[3,4,17], Christopher C Oakes[2,17], Ronald Simon[5,17], Katharina Grupp[5], Cristina Y Gerig[3], Dominik Bär[3], Mark D Robinson[6,7], Constance Baer[2], Melanie Weiss[2], Zuguang Gu[1], Matthieu Schapira[8], Ruprecht Kuner[9], Holger Sültmann[9], Maurizio Provenzano[10], ICGC Project on Early Onset Prostate Cancer[11], Marie-Laure Yaspo[12], Benedikt Brors[1], Jan Korbel[13], Thorsten Schlomm[14], Guido Sauter[5,18], Roland Eils[1,15,18], Christoph Plass[2,18] & Raffaella Santoro[3,18]

Prostate cancer is driven by a combination of genetic and/or epigenetic alterations. Epigenetic alterations are frequently observed in all human cancers, yet how aberrant epigenetic signatures are established is poorly understood. Here we show that the gene encoding BAZ2A (TIP5), a factor previously implicated in epigenetic rRNA gene silencing, is overexpressed in prostate cancer and is paradoxically involved in maintaining prostate cancer cell growth, a feature specific to cancer cells. BAZ2A regulates numerous protein-coding genes and directly interacts with EZH2 to maintain epigenetic silencing at genes repressed in metastasis. *BAZ2A* overexpression is tightly associated with a molecular subtype displaying a CpG island methylator phenotype (CIMP). Finally, high BAZ2A levels serve as an independent predictor of biochemical recurrence in a cohort of 7,682 individuals with prostate cancer. This work identifies a new aberrant role for the epigenetic regulator BAZ2A, which can also serve as a useful marker for metastatic potential in prostate cancer.

Prostate cancer is the most common non-cutaneous malignancy in men. Despite intensive research, prediction of clinical behavior remains challenging using the currently available histopathological and biochemical (prostate-specific antigen; PSA) markers; thus, novel molecular-based approaches will likely improve prognostic accuracy in this disease.

Cancer evolution is driven by a combination of genetic and epigenetic abnormalities; the crucial role of epigenetic gene regulation is indicated by the high frequency of mutations in key regulators of epigenetic marks, including DNA methylation[1–3]. As prostate cancer is characterized by a low frequency of somatic mutations[1], disruption of epigenetic pathways is likely to have an important role in the disease. Aberrant DNA methylation patterns are universally found in prostate cancer and are known to frequently affect genes involved in cancer-related processes[4–6]. An important contributor to altered epigenetic patterns in prostate cancer is enhancer of zeste homolog 2 (EZH2), whose altered expression is linked to malignancy and poor prognosis[7–11]. As the catalytic subunit of the Polycomb repressive complex (PRC2), EZH2 controls gene silencing by mediating trimethylation of histone H3 at lysine 27 (H3K27me3). Overexpression contributes to tumor development in part by leading to chromatin condensation and transcriptional repression of a broad range of genes involved in proliferation, invasion and angiogenesis[12–14].

In this work, we aimed to identify additional alterations to epigenetic regulators that contribute to poor prognosis in prostate cancer. We found that the epigenetic factor BAZ2A (also known as TIP5) is broadly overexpressed in prostate cancer. Alteration in BAZ2A levels is not caused by somatic structural or sequence variations but rather is likely due to post-transcriptional regulation involving loss of miR-133a. Interestingly, we found that BAZ2A cooperates with EZH2 to induce aberrant gene silencing in prostate cancer cell lines. BAZ2A overexpression is tightly associated with a prostate cancer subtype displaying CIMP in tumors and with prostate cancer recurrence in patients. Our results demonstrate that BAZ2A is a new biomarker that

[1]Division of Theoretical Bioinformatics, German Cancer Research Center (DKFZ), Heidelberg, Germany. [2]Division of Epigenomics and Cancer Risk Factors, German Cancer Research Center (DKFZ), Heidelberg, Germany. [3]Institute of Veterinary Biochemistry and Molecular Biology, University of Zurich, Zurich, Switzerland. [4]Molecular Life Science Program, Life Science Zurich Graduate School, University of Zurich, Zurich, Switzerland. [5]Institute of Pathology, University Medical Center Hamburg-Eppendorf, Hamburg, Germany. [6]Institute of Molecular Life Sciences, University of Zurich, Zurich, Switzerland. [7]Swiss Institute of Bioinformatics (SIB), University of Zurich, Zurich, Switzerland. [8]Department of Pharmacology and Toxicology, University of Toronto, Toronto, Ontario, Canada. [9]Unit of Cancer Genome Research, German Cancer Research Center (DKFZ) and National Center of Tumour Diseases, Heidelberg, Germany. [10]Oncology Research Unit, Division of Urology, University Hospital of Zurich, Zurich, Switzerland. [11]A list of contributing members and affiliations appears in the **Supplementary Note**. [12]Max Planck Institute for Molecular Genetics, Berlin, Germany. [13]Genome Biology Unit, European Molecular Biology Laboratory (EMBL), Heidelberg, Germany. [14]Martini Clinic, Prostate Cancer Center, University Medical Center Hamburg-Eppendorf, Hamburg, Germany. [15]Department for Bioinformatics and Functional Genomics, Institute for Pharmacy and Molecular Biotechnology (IPMB) and BioQuant, Heidelberg University, Heidelberg, Germany. [16]Present addresses: Department of Cell Biology, Harvard Medical School, Boston, Massachusetts, USA and Division of Newborn Medicine, Boston Children's Hospital, Boston, Massachusetts, USA. [17]These authors contributed equally to this work. [18]These authors jointly supervised this work. Correspondence should be addressed to R. Santoro (raffaella.santoro@vetbio.uzh.ch), C.P. (c.plass@dkfz-heidelberg.de), R.E. (r.eils@dkfz-heidelberg.de) or G.S. (g.sauter@uke.de).

Received 25 September; accepted 17 November; published online 8 December 2014; doi:10.1038/ng.3165

distinguishes aggressive disease and suggest a role for BAZ2A in the establishment of epigenetic alterations in aggressive prostate cancer.

RESULTS

BAZ2A is upregulated in prostate cancer

The low frequency of somatic mutations in prostate cancer prompted us to perform a focused search for epigenetic regulatory genes displaying altered expression in prostate cancer tumors. A recently defined list of 709 genes associated with epigenetic regulation[3] was interrogated in patient-matched tumor-normal expression data available from The Cancer Genome Atlas (TCGA) database[15] and in a second large data set containing 51 tumors and 48 normal samples (Brase data set)[16] (**Supplementary Table 1**). Genes showing altered expression (false discovery rate (FDR) $q < 0.05$) were ranked according to the degree of expression difference in each data set. This analysis identified consistent, high-ranking (within the top ten genes) overexpression of *BAZ2A* alongside other known epigenetic regulators with described roles in cancer, such as *PHF12*, *CHD6* and *EZH2*. Analysis of early-onset prostate cancer (EOPC) samples[2] provided further support for the overexpression of *BAZ2A* and *EZH2* (**Fig. 1a** and **Supplementary Table 1b**). BAZ2A (TIP5) is the largest subunit of the nucleolar remodeling complex NoRC, known to establish epigenetic silencing and transcriptional repression at rRNA genes (rDNA) through association with DNA methyltransferases and histone modifier complexes[17–19]. As upregulation of rRNA transcription is considered to contribute to malignant transformation and tumor cell proliferation[20,21], the upregulation of BAZ2A, a repressor of rDNA, is contradictory and peaked our further interest. *BAZ2A* levels were also increased in prostate cancer metastatic samples, whereas the expression of the polymerase I transcription factor *UBF* was not affected (**Fig. 1b** and **Supplementary Fig. 1a**). *BAZ2A* expression was again similar to that of *EZH2*, which was also increased in metastatic tumors[7] (**Fig. 1b**).

Analysis of genomic and DNA methylation data from 12 EOPC samples[2] did not demonstrate a genetic or epigenetic explanation for *BAZ2A* upregulation, with a lack of copy number alterations (CNAs), loss of heterozygosity, single-nucleotide variations, structural variations and promoter demethylation at the *BAZ2A* locus. The lack of mutations and CNAs was also verified in TCGA data (**Supplementary Fig. 2**), suggesting a post-transcriptional cause for aberrant *BAZ2A* expression in prostate cancer. *In silico* prediction of microRNAs (miRNAs) for *BAZ2A*[22] indicated that there was a high potential that miR-133a targets the 3′ UTR of this gene (**Supplementary Table 2**). miR-133a is known to function as a tumor suppressor in several cancer types[23–25] and has recently been reported to suppress cell proliferation, migration and invasion when expressed in prostate cancer cells[26,27]. We found that miR-133a levels were downregulated in the EOPC samples as well as in the TCGA and Brase data sets (**Fig. 1c**). In analysis of luciferase reporter constructs containing the *BAZ2A* 3′ UTR sequence, miR-133a expression mediated reduced luciferase levels (**Supplementary Fig. 1b**), whereas a reporter construct with a mutated miR-133a binding site in the *BAZ2A* 3′ UTR did not show reduced luciferase levels with miR-133a expression (**Fig. 1d**). Furthermore, miR-133a caused robust decreases in BAZ2A mRNA and protein levels, similar to those found using small interfering RNA (siRNA) targeting *BAZ2A* (**Fig. 1e** and **Supplementary Fig. 1c**). These data indicate that *BAZ2A* overexpression is typically not caused by somatic structural or sequence variations in prostate cancer but is rather likely due to post-transcriptional regulation involving loss of miR-133a.

BAZ2A paradoxically contributes to the proliferation and viability of metastatic prostate cancer cell lines

BAZ2A and its role in rDNA repression via the establishment of silent epigenetic marks has been studied so far only in non-malignant cells[17,19,28]; depletion of BAZ2A in NIH3T3 and COS cells caused

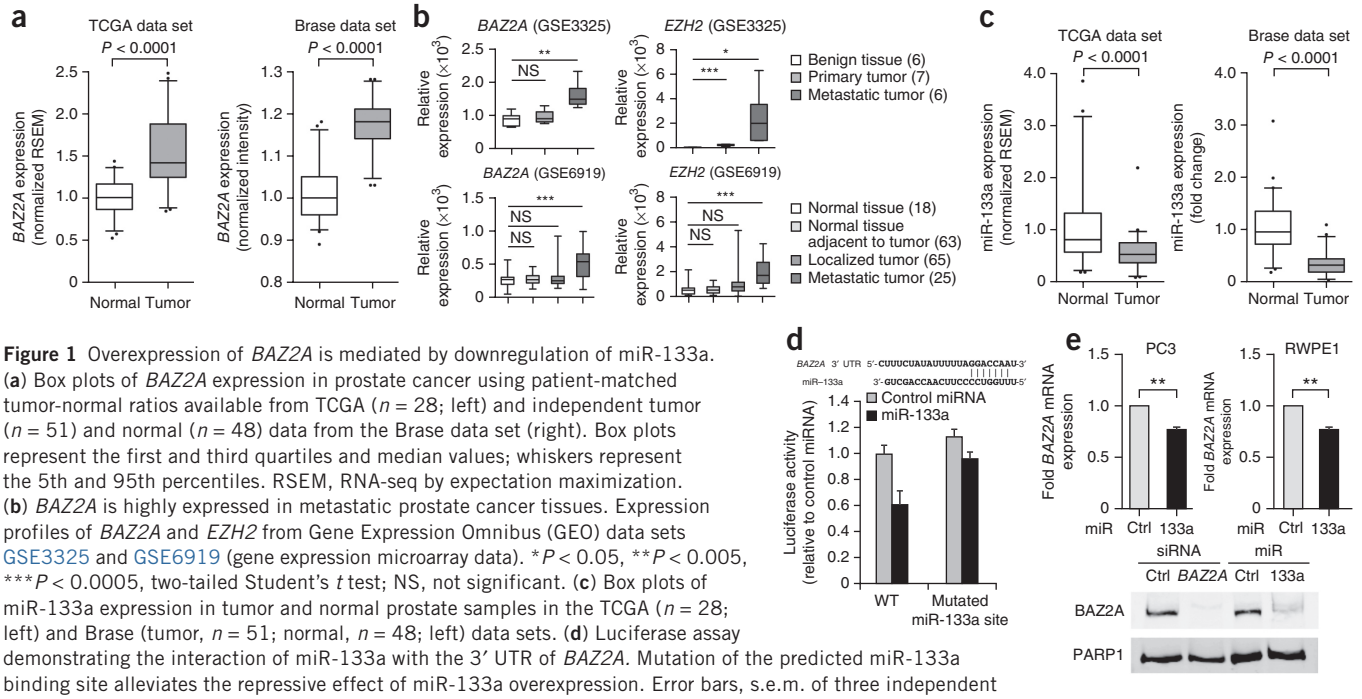

Figure 1 Overexpression of *BAZ2A* is mediated by downregulation of miR-133a. (**a**) Box plots of *BAZ2A* expression in prostate cancer using patient-matched tumor-normal ratios available from TCGA ($n = 28$; left) and independent tumor ($n = 51$) and normal ($n = 48$) data from the Brase data set (right). Box plots represent the first and third quartiles and median values; whiskers represent the 5th and 95th percentiles. RSEM, RNA-seq by expectation maximization. (**b**) *BAZ2A* is highly expressed in metastatic prostate cancer tissues. Expression profiles of *BAZ2A* and *EZH2* from Gene Expression Omnibus (GEO) data sets GSE3325 and GSE6919 (gene expression microarray data). $^*P < 0.05$, $^{**}P < 0.005$, $^{***}P < 0.0005$, two-tailed Student's *t* test; NS, not significant. (**c**) Box plots of miR-133a expression in tumor and normal prostate samples in the TCGA ($n = 28$; left) and Brase (tumor, $n = 51$; normal, $n = 48$; left) data sets. (**d**) Luciferase assay demonstrating the interaction of miR-133a with the 3′ UTR of *BAZ2A*. Mutation of the predicted miR-133a binding site alleviates the repressive effect of miR-133a overexpression. Error bars, s.e.m. of three independent experiments. WT, wild type. (**e**) miR-133a targets endogenous *BAZ2A*. Top, quantitative RT-PCR (qRT-PCR) of PC3 and RWPE1 cells transfected with miRNA-133a or control (Ctrl) miRNA. Data were normalized to *ACTB* mRNA levels. Bottom, BAZ2A immunoblot of nuclear extracts of PC3 cells transfected with the indicated siRNA or miRNA. $^{**}P < 0.005$, two-tailed Student's *t* test. Error bars, s.e.m. from three independent experiments.

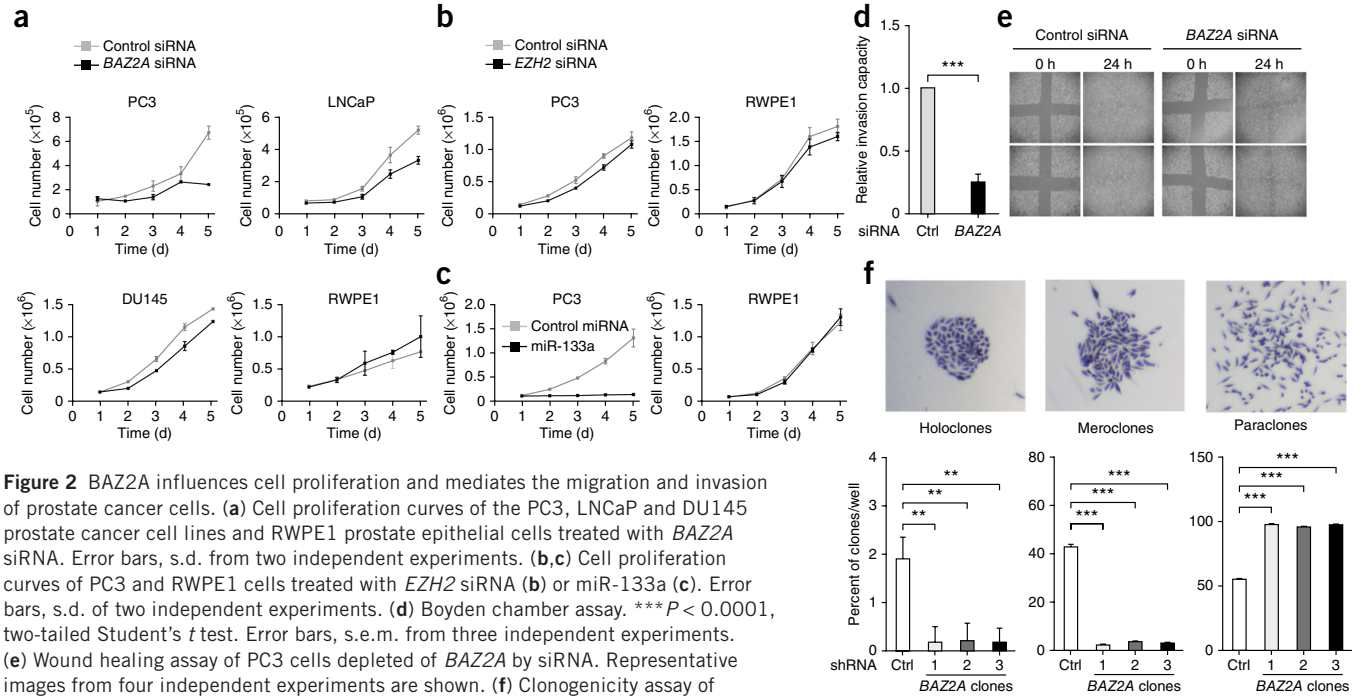

Figure 2 BAZ2A influences cell proliferation and mediates the migration and invasion of prostate cancer cells. (**a**) Cell proliferation curves of the PC3, LNCaP and DU145 prostate cancer cell lines and RWPE1 prostate epithelial cells treated with *BAZ2A* siRNA. Error bars, s.d. from two independent experiments. (**b**,**c**) Cell proliferation curves of PC3 and RWPE1 cells treated with *EZH2* siRNA (**b**) or miR-133a (**c**). Error bars, s.d. of two independent experiments. (**d**) Boyden chamber assay. $***P < 0.0001$, two-tailed Student's *t* test. Error bars, s.e.m. from three independent experiments. (**e**) Wound healing assay of PC3 cells depleted of *BAZ2A* by siRNA. Representative images from four independent experiments are shown. (**f**) Clonogenicity assay of PC3 cells stably expressing control short hairpin RNA (shRNA) or shRNA to *BAZ2A* (three distinct cell clones). Top, morphologies of holoclones, meroclones and paraclones isolated from PC3 cells. Bottom, frequency of each type of cell clone. $**P < 0.01$, $***P < 0.0001$, two-tailed Student's *t* test. Error bars, s.e.m. from three independent experiments.

loss of silencing epigenetic marks at rDNA, upregulation of rDNA transcription and an increase in ribosome production and cell proliferation, underscoring the intimate link between rRNA synthesis and cell proliferation[29,30]. Consistent with these previous findings, knockdown of *BAZ2A* by siRNA in normal prostate epithelial RWPE1 cells increased rDNA transcription and slightly enhanced cell proliferation (**Fig. 2a** and **Supplementary Fig. 1d–f**). *BAZ2A* depletion instead slowed proliferation rates and reduced rDNA transcription in all tested metastatic prostate cancer cell lines, including PC3, DU145 and LNCaP cells, although BAZ2A maintained its role in the epigenetic regulation of rDNA in PC3 cells. The unexpected downregulation of rDNA transcription upon *BAZ2A* knockdown might reflect the defective cell proliferation known to affect and modulate the activity of the rDNA transcription machinery[31]. The unusual phenotypes observed upon *BAZ2A* knockdown in metastatic prostate cancer cells suggest that the role of BAZ2A in prostate cancer cells extends beyond the epigenetic control of the rDNA locus. Similarly to *BAZ2A* knockdown, depletion of *EZH2* reduced the proliferation and viability of PC3 cells, underscoring the recognized oncogenic role of EZH2 in prostate cancer cells[7] (**Fig. 2b** and **Supplementary Fig. 1g**). Remarkably, addition of miR-133a drastically impaired the proliferation of PC3 cells, whereas RWPE1 cells remained unaffected (**Fig. 2c**).

No obvious changes in apoptosis and senescence were evident with *BAZ2A* knockdown in PC3 cells and in the non-malignant RWPE1 cell line (**Supplementary Fig. 3a**,**b**). However, cell cycle analysis showed an accumulation of PC3 cells in G1 phase after *BAZ2A* depletion, whereas no detectable changes were observed in RWPE1 cells (**Supplementary Fig. 3c**). In analysis of progression to S phase after the release of G1/S-synchronized PC3 cells, *BAZ2A* depletion induced a delay in progression in comparison to control PC3 cells and RWPE1 cells (**Supplementary Fig. 3d**). Consistent with these results, only PC3 cells with *BAZ2A* knockdown increased the expression of negative cell cycle regulators such as CDKN1A (**Supplementary Fig. 3e** and **Supplementary Tables 3** and **4**). Analysis of the invasion and migration of metastatic PC3 prostate cancer cells showed that these features of metastatic and aggressive prostate cancer were drastically impaired upon *BAZ2A* knockdown (**Fig. 2d**,**e**). Previous studies demonstrated that the PC3 cell line retains a small fraction of cells (~1%) that can initiate serially transplantable tumors[32,33] and can be distinguished by their ability to form holoclones, which are small, dense colonies with a high capacity for self-renewal[34,35]. Remarkably, unlike control knockdown cells, PC3 cells stably depleted of *BAZ2A* were unable to form holoclones and meroclones (an intermediate phenotype of holoclones) and generated only paraclones, which retain no self-renewal capacity (**Fig. 2f** and **Supplementary Fig. 3f**,**g**).

Taken together, these results indicate that, in contrast to its role in non-malignant cells, BAZ2A paradoxically contributes to the proliferation and viability of metastatic prostate cancer cell lines and is implicated in a cancer cell–specific phenotype involving migration, invasion and stem cell–like features of prostate cancer, which are important in metastasis and disease recurrence[36].

BAZ2A and EZH2 coordinate epigenetic silencing in prostate cancer cells

As the phenotypic analysis in prostate cancer cells suggested additional roles for BAZ2A that are rDNA independent, we reasoned that BAZ2A might regulate a class of non-rRNA genes that are critical for prostate cancer. Because of the various similarities between EZH2 and BAZ2A, we investigated global gene expression in PC3 prostate cancer cells depleted of *BAZ2A* or *EZH2* using microarrays. In this analysis, the transcription of 1,921 genes was significantly up- or downregulated after *BAZ2A* knockdown ($\log_2$ fold difference = 0.58; $P < 0.05$), whereas depletion of *EZH2* affected the expression of 1,793 genes (**Fig. 3a**,**b** and **Supplementary Table 3**). Remarkably, about one-third of the genes regulated by BAZ2A were also

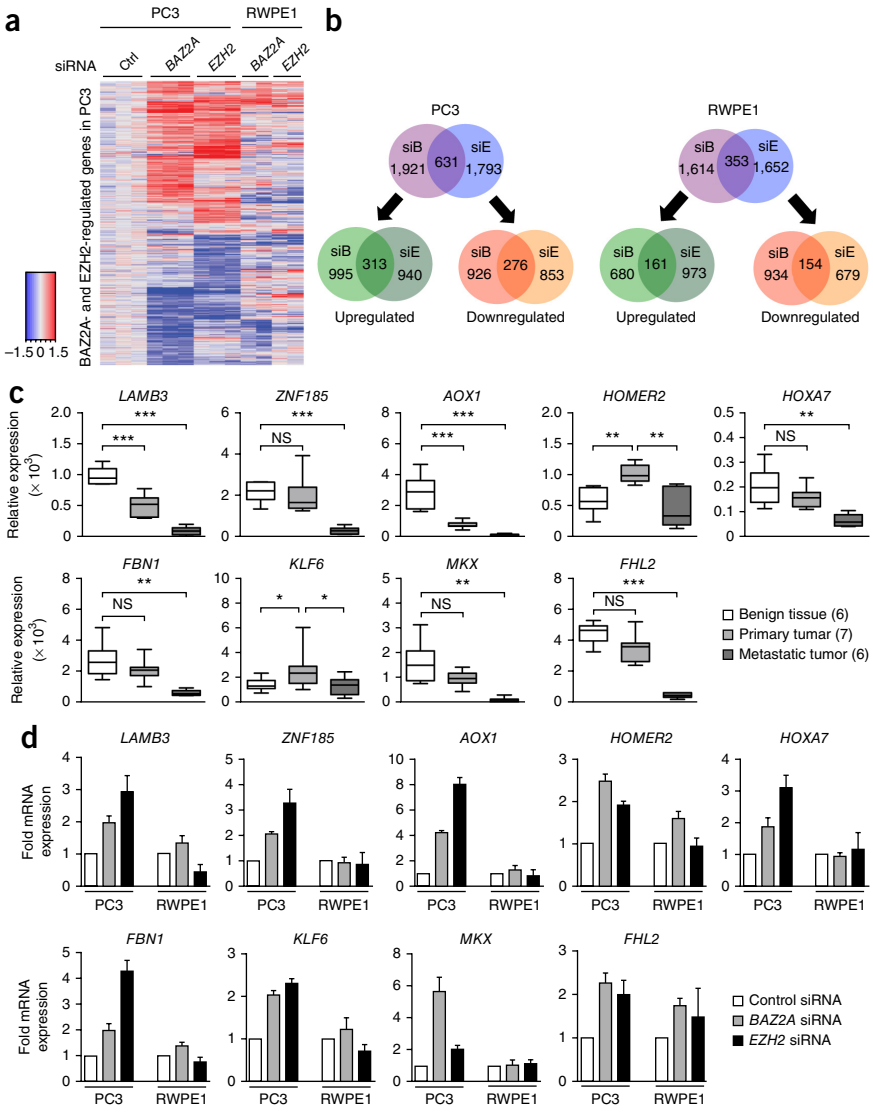

Figure 3 BAZ2A and EZH2 coordinate the repression of genes frequently silenced in metastatic prostate cancer. (**a**) Heat map of the expression levels of BAZ2A- and EZH2-regulated genes in PC3 and RWPE1 cells treated with the corresponding siRNAs. The heat map shows the $\log_2$ ratio relative to the average of the siRNA control samples.(**b**) Venn diagrams of BAZ2A- and EZH2-regulated genes in PC3 and RWPE1 cells treated with the corresponding siRNAs (siB, siRNA to *BAZ2A*; siE, siRNA to *EZH2*). The top diagram represents all genes regulated by BAZ2A or EZH2. The bottom diagrams refer to genes up- or downregulated in cells depleted of *BAZ2A* or *EZH2*. (**c**) Expression of eight RBEPM genes in benign tissue and primary and metastatic tumor tissues (GEO, GSE3325). $^*P < 0.05$, $^{**}P < 0.005$, $^{***}P < 0.0005$, two-tailed Student's *t* test; NS, not significant. (**d**) RBEPM genes are regulated by BAZ2A and EZH2 in PC3 but not RWPE1 cells. qRT-PCR showing the mRNA levels of RBEPMs in cells treated with siRNA to *BAZ2A* or *EZH2*. Data from two independent experiments were normalized to *ACTB* mRNA levels and to data for cells treated with control siRNA. Error bars, s.e.m. from three (PC3) and two (RWPE1) independent experiments.

regulated by EZH2, a proportion not expected by chance ($P = 2.2 \times 10^{-16}$, calculated by a combination of permutation and Fisher tests), indicating that BAZ2A and EZH2 regulate hundreds of genes in common in PC3 cells. In further support of an rDNA-independent role for BAZ2A in prostate cancer, abundant amounts of BAZ2A were present in the nucleoplasmatic fraction of PC3 cells (**Supplementary Fig. 4**), whereas all non-malignant mouse cells analyzed so far displayed an exclusive localization of BAZ2A within nucleoli, the nuclear compartment that contains rRNA genes (**Supplementary Fig. 4**). Gene set enrichment analysis (GSEA) uncovered a strong positive correlation with gene sets and pathways involved in metastasis (for example, extracellular matrix organization and collagen formation) and immune function (interferon and cytokine signaling) independently within both data sets ($q < 0.05$; **Supplementary Fig. 5** and **Supplementary Table 5**). Furthermore, the aging and senescence gene set that was recently found to be a signature for indolent prostate cancer[37] was negatively correlated with genes regulated by BAZ2A or EZH2 ($P < 0.01$ for both). In comparison to experiments in PC3 cells, knockdown of *BAZ2A* or *EZH2* in the non-malignant RWPE1 cell line resulted in an overlap of only 15% of genes, with only 16 of these genes having expression affected by both *BAZ2A* and *EZH2* knockdown in PC3 cells (**Fig. 3a**,**b** and **Supplementary Table 6**). Genes regulated by both BAZ2A and EZH2 in RWPE1 cells did not show any relevant gene ontology (GO) enrichment (**Supplementary Fig. 6**). Remarkably, the genes affected by *BAZ2A* depletion in PC3 and RWPE1 cells were implicated in distinct biological processes (**Supplementary Fig. 7**). Taken together, these data show that BAZ2A and EZH2 coordinate shared biological pathways in PC3 prostate cancer cells that are not present in non-malignant RWPE1 cells, suggesting a functional BAZ2A-EZH2 cooperation that is specific for metastatic prostate cancer cells.

To determine how the transcriptional repressors BAZ2A and EZH2 might cooperate to regulate genes with likely roles in prostate cancer metastasis, we identified 101 genes that were downregulated in metastatic tumors in comparison to normal prostate tissues or primary tumors[7,38] as well as upregulated upon *BAZ2A* or *EZH2* knockdown in PC3 cells. We termed these genes RBEPMs (repressed by BAZ2A and EZH2 in prostate cancer cells and repressed in metastatic prostate cancer tumors) (**Fig. 3c** and **Supplementary Table 3**). Upregulation of the nine RBEPMs (*AOX1*, *FBN1*, *FHL2*, *HOMER2*, *HOXA7*, *LAMB3*, *MKX*, *KLF6* and *ZNF185*) that showed the strongest downregulation in metastatic tumors (**Fig. 3c**) and had previously been reported to be hypermethylated and transcriptionally repressed in cancers[4,39–45] was validated in *BAZ2A* and *EZH2* knockdown cells (**Fig. 3d** and **Supplementary Fig. 8a**). Analysis of RWPE1 cells confirmed that these RBEPMs were predominantly not normally regulated by BAZ2A and EZH2 (**Fig. 3d** and **Supplementary Table 4**).

The substantial overlap of BAZ2A- and EZH2-regulated genes in PC3 cells prompted us to investigate the direct association and coordinated binding of BAZ2A and EZH2 at RBEPM promoters (**Fig. 3d**). Coimmunoprecipitation of Flag-HA-BAZ2A from the nuclear extracts of HEK293T cells showed an association with EZH2 (**Fig. 4a**). Chromatin immunoprecipitation (ChIP) analysis indicated

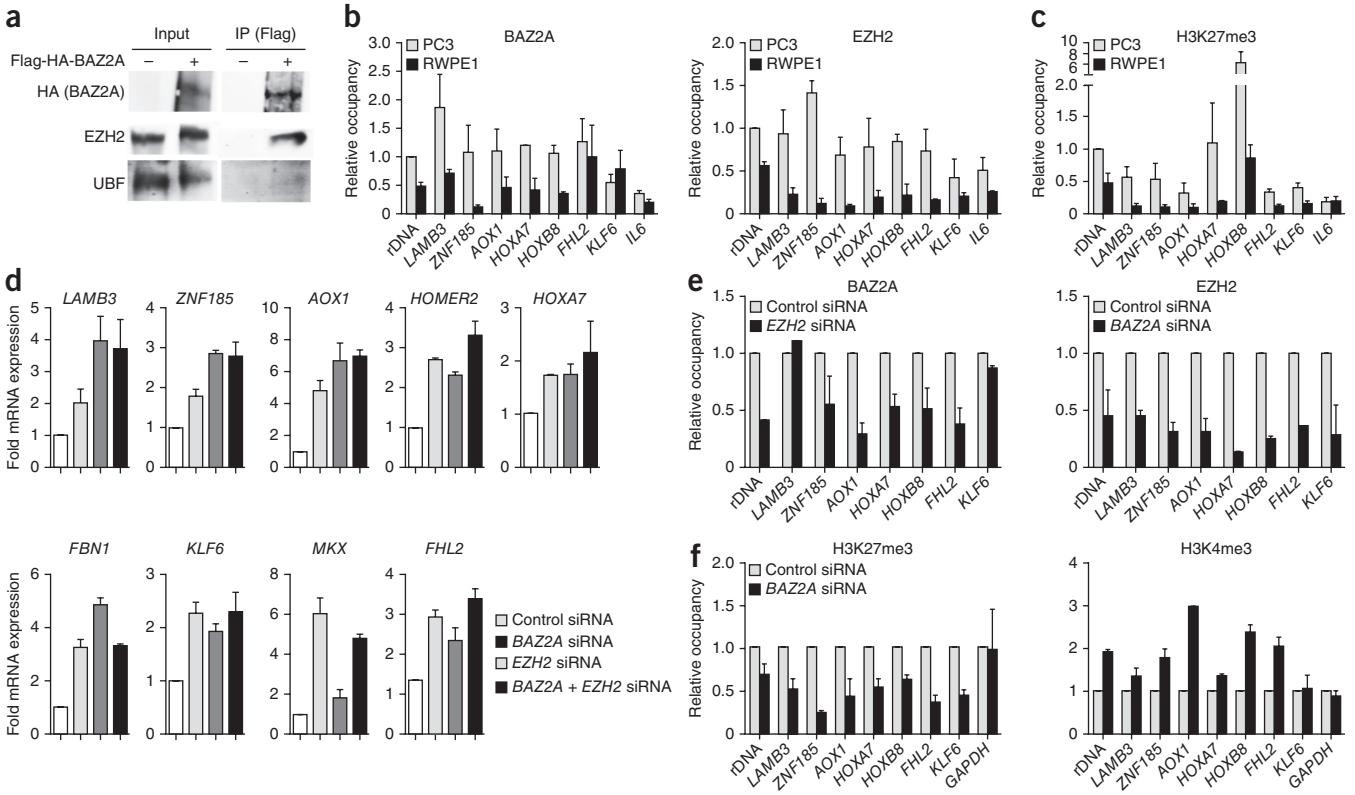

Figure 4 BAZ2A regulates aberrant epigenetic silencing in prostate cancer. (**a**) Flag-mediated immunoprecipitation of nuclear extracts from HEK293T cells expressing Flag-HA-BAZ2A. Immunoblots show the association of BAZ2A with EZH2. The specificity of immunoprecipitation was verified by the lack of immunoprecipitated UBF, which does not associate with BAZ2A. IP, immunoprecipitation. (**b**,**c**) BAZ2A and EZH2 levels (**b**) and H3K27me3 marks (**c**) are enriched at RBEPM gene promoters in PC3 cells. ChIP assays show associations with RBEPM promoters in PC3 and RWPE1 cells. Values are shown relative to input and to rDNA promoter sequences in PC3 cells. Error bars, s.e.m. from two independent experiments. (**d**) BAZ2A and EZH2 repress the transcription of RBEPM genes via a shared pathway. qRT-PCR of RBEPM transcripts from PC3 cells treated with siRNA to *BAZ2A*, *EZH2* or both. Error bars, s.e.m. from two independent experiments. (**e**) Recruitment of EZH2 to RBEPM promoters is interdependent with that of BAZ2A. ChIP analysis of the association of BAZ2A or EZH2 with RBEPM promoters in PC3 cells depleted of *EZH2* or *BAZ2A*, respectively. Data are shown relative to input and data for control cells. Error bars, s.e.m. from two independent experiments. (**f**) BAZ2A regulates H3K27me3 and H3K4me3 levels at RBEPMs in PC3 cells. ChIP of the indicated histone modifications. Data are shown relative to input and data for control cells. Error bars, s.e.m. from two independent experiments.

that BAZ2A and EZH2 were generally more associated with RBEPM and rDNA promoters in PC3 cells than in RWPE1 cells (**Fig. 4b**). Consistent with the BAZ2A and EZH2 binding profiles, H3K27me3 levels at RBEPM and rDNA promoter sequences were higher in PC3 cells than in RWPE1 cells, underscoring the role of histone repressive marks in transcriptional silencing at RBEPMs in prostate cancer cells (**Fig. 4c**). A lack of evident additive RBEPM activation upon combined depletion suggests that BAZ2A and EZH2 repress the transcription of RBEPM genes via a shared pathway (**Fig. 4d** and **Supplementary Fig. 8b**). Accordingly, all RBEPMs showed decreased association with EZH2 upon *BAZ2A* depletion (**Fig. 4e** and **Supplementary Fig. 8c**). Similar results were obtained for BAZ2A binding with the majority of RBEPMs (with the exception of *LAMB3* and *KLF6*) in PC3 cells in the absence of *EZH2*, indicating that the recruitment of EZH2 to RBEPM promoters is codependent on BAZ2A. Remarkably, depletion of *BAZ2A* decreased H3K27me3 levels and increased the association of the active histone mark H3K4me3 (trimethylation of histone H3 at lysine 4) with RBEPM and rDNA promoter sequences (**Fig. 4f**). Taken together, the results show the essential role of BAZ2A in coordinating EZH2 recruitment and the establishment of H3K27 methylation at genes frequently repressed in metastatic prostate cancer. The data indicate that BAZ2A acts as epigenetic regulator for the transcriptional repression of genes that are implicated in aggressive prostate cancer.

Tumors with high BAZ2A expression display a CpG island hypermethylator phenotype

Because BAZ2A is known to interact with DNA methyltransferases and this association is required to establish epigenetic silencing at rDNA in all cells[17], we next investigated whether the upregulation of BAZ2A was associated with altered DNA methylation in prostate tumors. As we determined that BAZ2A was primarily regulated post-transcriptionally, we analyzed BAZ2A protein levels in prostate tumors and normal tissues using immunohistochemistry on a tissue microarray (TMA) of 384 samples. BAZ2A immunostaining was variable between prostate tumor specimens in comparison to normal prostate epithelium, with strong and weak staining in 21% and 25% of samples, respectively. We selected 22 tumors with high BAZ2A protein levels and 13 tumors with low BAZ2A protein levels for DNA methylation analysis using the Illumina Infinium HumanMethylation450 (450K) array. Samples were also selected to have >70% tumor content, which was confirmed to not appreciably differ between samples with high and low BAZ2A expression by observing between the groups consistent hypermethylation of *GSTP1* (ref. 46) and *APC*[47], genes known to

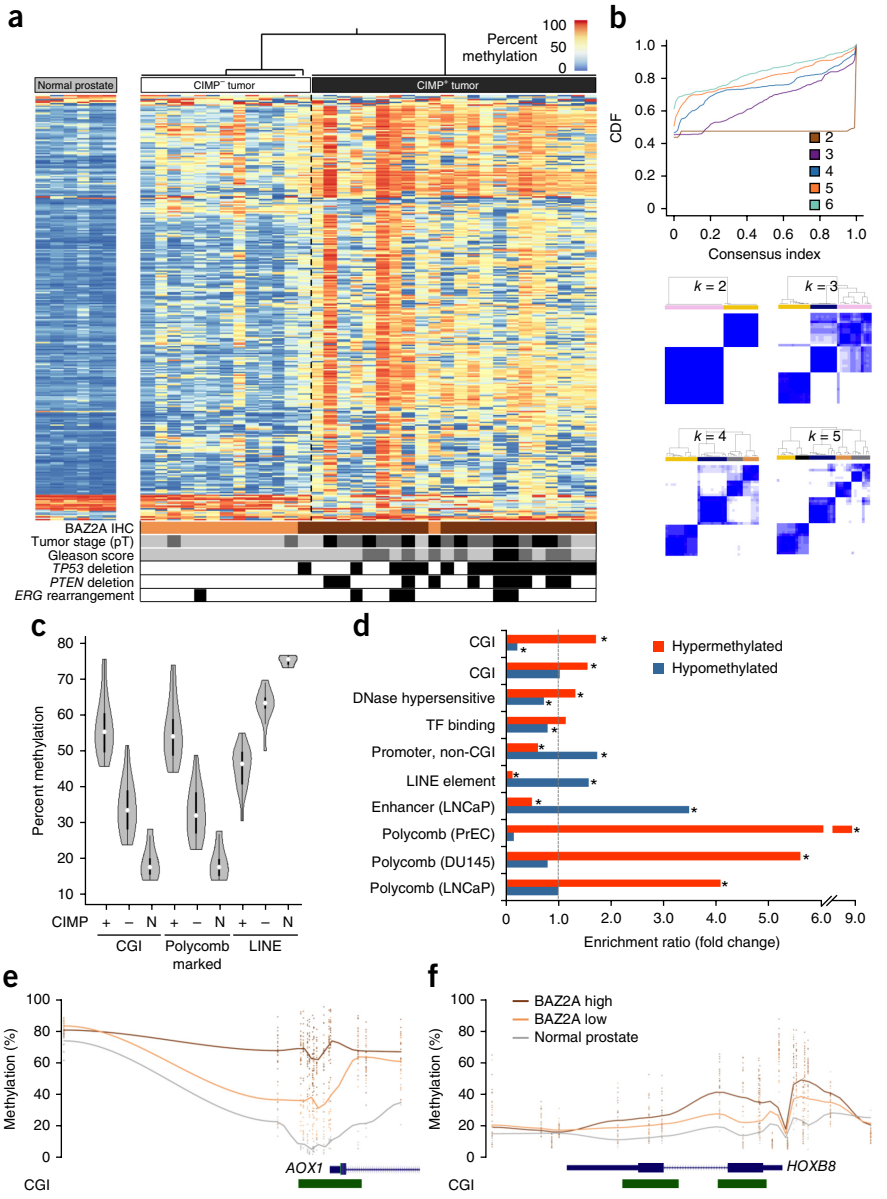

Figure 5 Epigenetic remodeling in prostate tumors overexpressing BAZ2A. (**a**) A heat map of the DNA methylation values of the 3,000 most variable CpG sites from 450K array analysis. Hierarchical clustering of tumors identifies two DNA methylation subtypes displaying relatively high and low levels of methylation (termed CIMP$^+$ and CIMP$^-$, respectively). Tumors displaying high and low levels of BAZ2A from immunohistochemical (IHC) evaluation are represented by dark and light brown color, respectively. Increasing tumor stage (pT2, pT3a and pT3b) and Gleason score (3+4, 4+3 and ≥4+4) are illustrated by an increase in shading intensity from light gray to dark gray to black for the corresponding indicators. The presence of *TP53* and *PTEN* deletions, as well as *ERG* rearrangements, is indicated. (**b**) Top, cumulative distribution function (CDF) for class numbers ranging from two to six. Bottom, consensus clustering heat maps of the consensus matrices for class numbers ranging from two to five. (**c**) DNA methylation levels of CGIs, Polycomb-marked regions and LINE elements in CIMP$^+$ and CIMP$^-$ tumors and in normal tissue (N) show methylation features consistent with previously defined CIMP phenotypes (white dots indicate the median, boxes indicate the interquartile range). (**d**) Enrichment and/or depletion of genomic features in tumors with high versus low BAZ2A expression. Annotations of enhancer and Polycomb features were derived from ChIP sequencing profiles for LNCaP, DU145 and PrEC cells. (TF, transcription factor; PrEC, prostate epithelial cells). *$P < 0.001$. (**e**,**f**) DNA methylation profiles of the promoter regions of the RBEPM genes *AOX1* (**e**) and *HOXB8* (**f**) in tumor subtypes with high and low BAZ2A expression versus normal prostate tissue.

be hypermethylated in early disease stages (**Supplementary Fig. 9a**). Genome-wide analysis showed that the methylation of 32,707 CpGs was significantly altered (by more than ±20%; $q < 0.05$) in comparison to 6 normal prostate samples, with 24,497 and 8,210 CpGs hyper- and hypomethylated, respectively (**Fig. 5a**). Unsupervised clustering of the 3,000 most variable of these CpGs identified 2 distinct DNA methylation subtypes. A statistical evaluation showed an optimal number of two distinct methylation subtypes (**Fig. 5b**). To validate this finding, we independently interrogated TCGA prostate cancer data using the same approach of separating samples into those with high versus low BAZ2A expression (on the basis of available RNA expression data) and identifying *de novo* the 3,000 most variable probes (**Supplementary Fig. 10**). Ninety percent of the most variable CpGs were common to both analyses and furthermore identified two distinct methylation subgroups. One of the subtypes was characterized by a higher degree of hypermethylation of CpG islands (CGIs) and sites associated with Polycomb repression (as defined in LNCaP cells[48]) while simultaneously demonstrating hypomethylation of repetitive elements (such as long interspersed nuclear elements, LINEs) (**Fig. 5c**). The pattern present in this subtype is reminiscent of a CGI hypermethylator phenotype (CIMP) observed in other cancers[49–51], as well as globally in prostate cancer[5,52]. We observed a striking correlation between BAZ2A expression levels and the CIMP subtype, with 21 of 22 CIMP-positive samples displaying high BAZ2A levels and 12 of 13 normal-like samples exhibiting low BAZ2A levels. We also observed a similar association of the CIMP subtype with high BAZ2A expression in the analysis of TCGA data (**Supplementary Fig. 10**). Comparing tumors with high and low BAZ2A expression, in the subtype with high expression, 6,155 CpGs were hypermethylated and 1,679 CpGs were hypomethylated (difference in methylation of greater than ±20%). Hypermethylated CpGs were enriched in transcription factor binding and DNase-hypersensitive sites in addition to CGIs and CGI shore regions (**Fig. 5d**). Hypermethylation in tumors with high BAZ2A levels was strongly enriched in Polycomb-silenced regions (as defined in DU145 and LNCaP cells or primary prostate epithelial cells). Thus, elevated BAZ2A levels are associated with widespread epigenetic remodeling that includes functional regions, such as promoter and enhancer regions, and with Polycomb-associated domains. Considering our findings connecting BAZ2A with EZH2 and H3K27me3 in PC3 prostate cancer cells, the observation of greater hypermethylation of H3K27me3-marked regions suggests that high BAZ2A overexpression might be involved in the

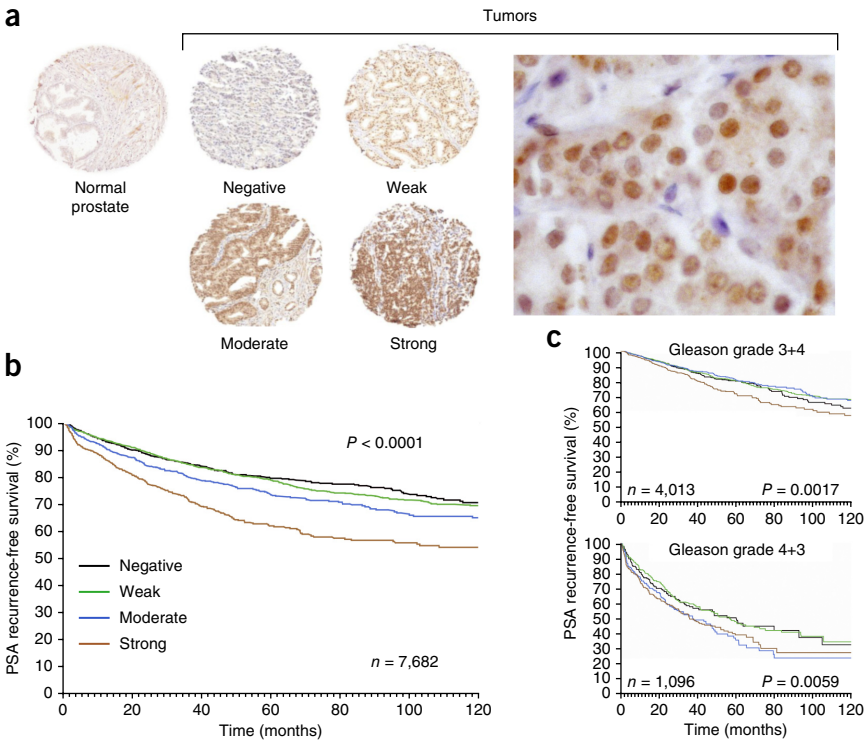

Figure 6 TMA and clinical evaluation of BAZ2A levels in 7,682 prostate tumor specimens. (**a**) Representative examples of TMA histological sections showing normal prostate and the negative, weak, moderate and strong BAZ2A staining classifications. Enhanced magnification (400×) of a representative tumor sample is shown (right). (**b**) Kaplan-Maier analysis of the time to postoperative PSA recurrence versus BAZ2A levels in all prostate tumors. *P* values were obtained by log-rank test (BAZ2A negative, $n = 1,998$; BAZ2A weak, $n = 2,809$; BAZ2A moderate, $n = 1,419$; BAZ2A strong, $n = 1,456$). (**c**) Cases were subdivided by Gleason grade to assess the capacity of BAZ2A levels to predict the frequency of postoperative PSA recurrence. Cases classified as low risk (3+4; top) and intermediate risk (4+3; bottom) display an increased likelihood of recurrence with increasing BAZ2A levels. Gleason grade 3+4: BAZ2A negative, $n = 1,036$; BAZ2A weak, $n = 1,461$; BAZ2A moderate, $n = 777$; BAZ2A strong, $n = 739$. Gleason grade 4+3: BAZ2A negative, $n = 211$; BAZ2A weak, $n = 353$; BAZ2A moderate, $n = 213$; BAZ2A strong, $n = 319$.

establishment of abnormal methylation patterns in prostate tumors. Tumors with high BAZ2A levels were also associated with advanced tumor stages and higher Gleason scores.

BAZ2A-associated alterations to DNA methylation were found to involve numerous genes and pathways that are known to be associated with prostate cancer in general (**Supplementary Table 7**), including hypermethylation of prostate cancer–relevant gene promoters and miRNAs known to inhibit androgen receptor expression[53–58] (**Supplementary Fig. 9b**,**c**). In comparison to the genes that become derepressed following *BAZ2A* knockdown in PC3 cells, 352 genes (35%) were found to have elevated levels of DNA methylation in tumors with high versus low BAZ2A expression, a number greater than expected by chance ($P = 0.0029$). There were 27 genes that were hypermethylated in tumors with high BAZ2A levels and upregulated upon both *BAZ2A* or *EZH2* knockdown in PC3 cells (**Fig. 5e**,**f**). Next, we performed GSEA on genes with differential promoter methylation in tumors with high and low BAZ2A levels (**Supplementary Fig. 11** and **Supplementary Tables 7** and **8**). Several cellular pathways and functions that are relevant to cancer development were found to be significantly enriched (FDR $q < 0.05$), including cell growth (cell cycle and transcription pathways) and genome stability (chromosome and telomere maintenance pathways). These gene sets were also identified for the genes showing differential expression with *BAZ2A* knockdown in PC3 cells (**Supplementary Fig. 5**). Moreover, hypermethylated genes in tumors with high BAZ2A levels and genes derepressed upon *BAZ2A* depletion in PC3 cells showed identical GO terms (**Supplementary Fig. 12**). Taken together, the data support a functional role for BAZ2A in DNA hypermethylation in prostate cancer tumors (**Supplementary Fig. 12**).

BAZ2A levels predict PSA recurrence in individuals with prostate cancer

We investigated the potential clinical relevance of BAZ2A in prostate cancer using a large TMA. This analysis included 7,682 informative samples for which clinical follow-up data were available. Case characteristics and clinical data are displayed in **Supplementary Table 9**. BAZ2A immunostaining in tumor samples was categorized as negative (26.1%), weak (36.7%), moderate (18.5%) or strong (19.0%) (as in **Fig. 5**; examples shown in **Fig. 6a**). We observed nuclear localization of BAZ2A, including increased staining in nucleoli (**Fig. 6a** and **Supplementary Fig. 13**). Strong BAZ2A staining was highly associated with advanced prostate tumor stage, high Gleason grade, the presence of lymph node metastasis, high preoperative PSA levels and positive surgical margin when considering all tumors or following subgrouping by *ERG* rearrangement status ($P < 0.0001$ for each; **Supplementary Table 10a–c**). The time to postoperative PSA recurrence was significantly shorter in the group with strong BAZ2A expression ($P < 0.0001$; **Fig. 6b**). Using Cox regression multivariate analysis to determine the relative dependence of recurrence on several prognostic and surgical parameters, the level of BAZ2A was determined to be independently predictive of PSA recurrence in multiple scenarios ($P < 0.0001$; **Supplementary Table 11a–c**). The independent predictive power of BAZ2A was further upheld following subdivision of the cases by *ERG* rearrangement status ($P < 0.0001$; **Supplementary Fig. 14**). Notably, to answer the question of whether BAZ2A levels could be used as a marker to aid in preoperative therapy decision-making for low- and intermediate-risk cases, we subdivided the cases by Gleason score and compared the frequency of postoperative PSA recurrence. BAZ2A levels were significantly predictive of PSA recurrence in cases with a Gleason score of 3+4 (low-intermediate risk; $n = 4,013$, $P = 0.0017$) or 4+3 (high-intermediate risk; $n = 1,096$, $P = 0.0059$) (**Fig. 6c**). BAZ2A levels did not show significant predictive ability in cases with a Gleason score of ≤3+3 (indolent prostate cancer; $n = 1,690$), likely owing to the occurrence of relatively very few events in this group, nor in very high-risk cases (Gleason score of ≥4+4; $n = 322$) (**Supplementary Fig. 14**). These results demonstrate a clear association of BAZ2A levels in prostate cancer tumor samples with PSA recurrence that is independent of standard prognostic and surgical parameters and can distinguish cases that

are ore likely to recur in the most uncertain group of individuals at intermediate risk.

DISCUSSION

Alterations involving epigenetic regulators are now recognized as key events governing the tumor cell phenotype by affecting the expression of genes critical to cancer. This work identified a new aberrant epigenetic signature (CIMP) that distinguishes prostate cancer tumors with high and low BAZ2A expression. Elevated BAZ2A levels associate with poor prognosis and disease recurrence, and tumors with high BAZ2A expression contain a specific set of hypermethylated genes implicated in several pathways relevant to cancer. We provide multiple lines of evidence that support the role of BAZ2A in the establishment of epigenetic alterations in cases with poor prognosis. Through the combined analysis of metastatic prostate cancer cell lines and tumor samples from patients, we found that the role of BAZ2A in prostate cancer goes beyond the epigenetic control of the rDNA locus. Using prostate cancer cell lines, we show that BAZ2A regulates genes (i) frequently repressed in metastatic prostate cancer and (ii) hypermethylated in prostate cancer cases with poor prognosis. The analysis of hypermethylated sequences in tumors with high BAZ2A expression identified an enrichment of sites associated with Polycomb repression that is in agreement with the results from the prostate cancer cell line describing the repression activity of BAZ2A in concert with Polycomb-based silencing. Furthermore, genes regulated by BAZ2A in prostate cancer cell lines and hypermethylated in tumors with high BAZ2A levels involve similar pathways and cancer-related processes. A role for BAZ2A in establishing epigenetic alterations that might favor the aggressive prostate cancer phenotype is also supported by the phenotypic analysis in prostate cancer cell lines showing an impact of BAZ2A on cancer-specific features such as proliferation, migration and invasion. Future studies will aim to define how and at which time point in prostate cancer progression BAZ2A exerts its oncogenic effect. Notably, we showed that high expression of BAZ2A in prostate cancer is likely caused by post-transcriptional regulation, supporting the idea that the disruption of epigenetic pathways is likely to have an important role in this disease.

Lethality in prostate cancer is linked to the evolution of a metastatic phenotype. PSA recurrence following radical prostatectomy signifies that tumor cells gained the ability to invade surrounding tissues and/or metastasize before surgery. Our results suggest that high BAZ2A levels in the primary tumor indicate a higher probability of metastasis, linking molecular findings with recurrence in clinical samples. We have shown BAZ2A levels to be an independent prognostic marker of recurrence, especially in low- and intermediate-risk cases, as assessed by Gleason score. Intermediate-risk cases are a subcohort with the most uncertainty in deciding the right balance between active surveillance and immediate definite therapy to avoid overtreatment. Screening of BAZ2A levels in biopsies might be a valuable biomarker to distinguish prostate cancer that may progress, aiding in the therapy decision-making for this important patient subgroup. Additionally, as an increasing number of epigenetic regulators, including members of the bromodomain-containing protein class, are currently being found to be dysregulated across many cancer types[59], BAZ2A, which contains a bromodomain required for its silencing function at rDNA[60], might represent a promising therapeutic target for metastatic prostate cancer.

URLs. TCGA Data Portal, https://tcga-data.nci.nih.gov/tcga/dataAccessMatrix.htm; Database for Annotation, Visualization and Integrated Discovery (DAVID), http://david.abcc.ncifcrf.gov/; miRGator v3.0, http://mirgator.kobic.re.kr/; Gene Set Enrichment Analysis (GSEA), http://www.broadinstitute.org/gsea/.

METHODS

Methods and any associated references are available in the online version of the paper.

Accession codes. The 450K array data can be found at the European Genome-phenome Archive (EGA) under accession EGAS00001000568.

Note: Any Supplementary Information and Source Data files are available in the online version of the paper.

ACKNOWLEDGMENTS

We acknowledge the entire team of the German ICGC Project on Early Onset Prostate Cancer. We thank M. Lupien, C. Schmidt, D. Wuttig, O. Bogatyrova, A. Postępska-Igielska and N. Schmitt for assistance with experiments and data. This project was supported by the German Federal Ministry of Education and Science in the Program for Medical Genome Research including the EOPC project within ICGC (FKZ; 01KU1001A, 01KU1001B, 01KU1001C, 01KU1001D and 01GS0890), by Krebsforschung Schweiz (KFS; 02732-02-2011), by the Swiss National Science Foundation (SNF; 310003A-135801 and 31003A-152854), by Swiss Life, by a Müller Molecular Life Science fellowship and by Mäxi Stiftung. We acknowledge assistance provided by the Genomics and Proteomics Core Facility at the German Cancer Research Center. In particular, we acknowledge the excellent technical support of M. Schick.

AUTHOR CONTRIBUTIONS

L.G., S.C.F., C.C.O., R. Simon, K.G., C.Y.G., D.B., M.P., C.B., M.W. and R.K. designed the experiments and performed experimental work. L.G., R.E., C.C.O., R. Simon, Z.G., R.K., M.D.R., M.S. and K.G. performed data analysis. R.K., G.S. and H.S. provided clinical samples or data. L.G., S.C.F., C.C.O., R. Simon, C.P., G.S., R.E. and R. Santoro prepared the manuscript and figures. M.-L.Y., B.B., J.K., T.S., G.S., R.E., H.S., C.P. and R. Santoro provided project leadership. All authors contributed to the final manuscript.

COMPETING FINANCIAL INTERESTS

The authors declare no competing financial interests.

1. Grasso, C.S. *et al.* The mutational landscape of lethal castration-resistant prostate cancer. *Nature* **487**, 239–243 (2012).
2. Weischenfeldt, J. *et al.* Integrative genomic analyses reveal an androgen-driven somatic alteration landscape in early-onset prostate cancer. *Cancer Cell* **23**, 159–170 (2013).
3. Plass, C. *et al.* Mutations in regulators of the epigenome and their connections to global chromatin patterns in cancer. *Nat. Rev. Genet.* **14**, 765–780 (2013).
4. Kim, J.H. *et al.* Deep sequencing reveals distinct patterns of DNA methylation in prostate cancer. *Genome Res.* **21**, 1028–1041 (2011).
5. Kron, K. *et al.* Altered DNA methylation landscapes of polycomb-repressed loci are associated with prostate cancer progression and *ERG* oncogene expression in prostate cancer. *Clin. Cancer Res.* **19**, 3450–3461 (2013).
6. Aryee, M.J. *et al.* DNA methylation alterations exhibit intraindividual stability and interindividual heterogeneity in prostate cancer metastases. *Sci. Transl. Med.* **5**, 169ra10 (2013).
7. Varambally, S. *et al.* The polycomb group protein EZH2 is involved in progression of prostate cancer. *Nature* **419**, 624–629 (2002).
8. Bracken, A.P. *et al. EZH2* is downstream of the pRB-E2F pathway, essential for proliferation and amplified in cancer. *EMBO J.* **22**, 5323–5335 (2003).
9. Hinz, S. *et al.* Expression of the polycomb group protein EZH2 and its relation to outcome in patients with urothelial carcinoma of the bladder. *J. Cancer Res. Clin. Oncol.* **134**, 331–336 (2008).
10. Bachmann, I.M. *et al.* EZH2 expression is associated with high proliferation rate and aggressive tumor subgroups in cutaneous melanoma and cancers of the endometrium, prostate, and breast. *J. Clin. Oncol.* **24**, 268–273 (2006).
11. Kleer, C.G. *et al.* EZH2 is a marker of aggressive breast cancer and promotes neoplastic transformation of breast epithelial cells. *Proc. Natl. Acad. Sci. USA* **100**, 11606–11611 (2003).
12. Crea, F., Paolicchi, E., Marquez, V.E. & Danesi, R. Polycomb genes and cancer: time for clinical application? *Crit. Rev. Oncol. Hematol.* **83**, 184–193 (2012).
13. Tsang, D.P. & Cheng, A.S. Epigenetic regulation of signaling pathways in cancer: role of the histone methyltransferase EZH2. *J. Gastroenterol. Hepatol.* **26**, 19–27 (2011).

14. Richly, H., Aloia, L. & Di Croce, L. Roles of the Polycomb group proteins in stem cells and cancer. *Cell Death Dis.* **2**, e204 (2011).
15. Cancer Genome Atlas Research Network. Comprehensive genomic characterization defines human glioblastoma genes and core pathways. *Nature* **455**, 1061–1068 (2008).
16. Brase, J.C. *et al. TMPRSS2-ERG*–specific transcriptional modulation is associated with prostate cancer biomarkers and TGF-β signaling. *BMC Cancer* **11**, 507 (2011).
17. Santoro, R., Li, J. & Grummt, I. The nucleolar remodeling complex NoRC mediates heterochromatin formation and silencing of ribosomal gene transcription. *Nat. Genet.* **32**, 393–396 (2002).
18. Zhou, Y., Santoro, R. & Grummt, I. The chromatin remodeling complex NoRC targets HDAC1 to the ribosomal gene promoter and represses RNA polymerase I transcription. *EMBO J.* **21**, 4632–4640 (2002).
19. Guetg, C., Scheifele, F., Rosenthal, F., Hottiger, M.O. & Santoro, R. Inheritance of silent rDNA chromatin is mediated by PARP1 via noncoding RNA. *Mol. Cell* **45**, 790–800 (2012).
20. Hein, N., Hannan, K.M., George, A.J., Sanij, E. & Hannan, R.D. The nucleolus: an emerging target for cancer therapy. *Trends Mol. Med.* **19**, 643–654 (2013).
21. Bywater, M.J. *et al.* Inhibition of RNA polymerase I as a therapeutic strategy to promote cancer–specific activation of p53. *Cancer Cell* **22**, 51–65 (2012).
22. Cho, S. *et al.* MiRGator v3.0: a microRNA portal for deep sequencing, expression profiling and mRNA targeting. *Nucleic Acids Res.* **41**, D252–D257 (2013).
23. Dong, Y.J. *et al.* MiR-133a inhibits colorectal cancer cell growth by direct targeting E3 ubiquitin ligase RFFL and activating p53-p21CIP1/WAF1 pathway. *Gastroenterology* **142**, S185 (2012).
24. Uchida, Y. *et al.* MiR-133a induces apoptosis through direct regulation of GSTP1 in bladder cancer cell lines. *Urol. Oncol.* **31**, 115–123 (2013).
25. Ji, F. *et al.* MicroRNA-133a, downregulated in osteosarcoma, suppresses proliferation and promotes apoptosis by targeting Bcl-xL and Mcl-1. *Bone* **56**, 220–226 (2013).
26. Tao, J. *et al.* MicroRNA-133 inhibits cell proliferation, migration and invasion in prostate cancer cells by targeting the epidermal growth factor receptor. *Oncol. Rep.* **27**, 1967–1975 (2012).
27. Kojima, S. *et al.* Tumor suppressors miR-1 and miR-133a target the oncogenic function of purine nucleoside phosphorylase (*PNP*) in prostate cancer. *Eur. Urol. Suppl.* **106**, 405–413 (2012).
28. Li, J., Santoro, R., Koberna, K. & Grummt, I. The chromatin remodeling complex NoRC controls replication timing of rRNA genes. *EMBO J.* **24**, 120–127 (2005).
29. Santoro, R., Lienemann, P. & Fussenegger, M. Epigenetic engineering of ribosomal RNA genes enhances protein production. *PLoS ONE* **4**, e6653 (2009).
30. Guetg, C. *et al.* The NoRC complex mediates the heterochromatin formation and stability of silent rRNA genes and centromeric repeats. *EMBO J.* **29**, 2135–2146 (2010).
31. Grummt, I. Life on a planet of its own: regulation of RNA polymerase I transcription in the nucleolus. *Genes Dev.* **17**, 1691–1702 (2003).
32. Li, H., Chen, X., Calhoun-Davis, T., Claypool, K. & Tang, D.G. PC3 human prostate carcinoma cell holoclones contain self-renewing tumor-initiating cells. *Cancer Res.* **68**, 1820–1825 (2008).
33. Sheng, X. *et al.* Isolation and enrichment of PC-3 prostate cancer stem-like cells using MACS and serum-free medium. *Oncol. Lett.* **5**, 787–792 (2013).
34. Zhang, K. & Waxman, D.J. PC3 prostate tumor–initiating cells with molecular profile FAM65B^{high}/MFI2^{low}/LEF1^{low} increase tumor angiogenesis. *Mol. Cancer* **9**, 319 (2010).
35. Doherty, R.E., Haywood-Small, S.L., Sisley, K. & Cross, N.A. Aldehyde dehydrogenase activity selects for the holoclone phenotype in prostate cancer cells. *Biochem. Biophys. Res. Commun.* **414**, 801–807 (2011).
36. Collins, A.T., Berry, P.A., Hyde, C., Stower, M.J. & Maitland, N.J. Prospective identification of tumorigenic prostate cancer stem cells. *Cancer Res.* **65**, 10946–10951 (2005).
37. Irshad, S. *et al.* A molecular signature predictive of indolent prostate cancer. *Sci. Transl. Med.* **5**, 202ra122 (2013).
38. Yu, Y.P. *et al.* Gene expression alterations in prostate cancer predicting tumor aggression and preceding development of malignancy. *J. Clin. Oncol.* **22**, 2790–2799 (2004).
39. Wang, Y. *et al.* Survey of differentially methylated promoters in prostate cancer cell lines. *Neoplasia* **7**, 748–760 (2005).
40. Mori, Y. *et al.* Novel candidate colorectal cancer biomarkers identified by methylation microarray-based scanning. *Endocr. Relat. Cancer* **18**, 465–478 (2011).
41. Kinoshita, M., Nakagawa, T., Shimizu, A. & Katsuoka, Y. Differently regulated androgen receptor transcriptional complex in prostate cancer compared with normal prostate. *Int. J. Urol.* **12**, 390–397 (2005).
42. Novak, P. *et al.* Epigenetic inactivation of the *HOXA* gene cluster in breast cancer. *Cancer Res.* **66**, 10664–10670 (2006).
43. Zhang, J.S., Gong, A. & Young, C.Y. ZNF185, an actin-cytoskeleton-associated growth inhibitory LIM protein in prostate cancer. *Oncogene* **26**, 111–122 (2007).
44. Cheng, X.F. *et al.* Growth inhibitory effect of Kruppel-like factor 6 on human prostatic carcinoma and renal carcinoma cell lines. *Tohoku J. Exp. Med.* **216**, 35–45 (2008).
45. Wang, N. *et al.* Screening and identification of distant metastasis-related differentially expressed genes in human squamous cell lung carcinoma. *Anat. Rec. (Hoboken)* **295**, 748–757 (2012).
46. Maksimovic, J., Gordon, L. & Oshlack, A. SWAN: subset-quantile within array normalization for Illumina Infinium HumanMethylation450 BeadChips. *Genome Biol.* **13**, R44 (2012).
47. Lee, W.H. *et al.* Cytidine methylation of regulatory sequences near the π-class glutathione S-transferase gene accompanies human prostatic carcinogenesis. *Proc. Natl. Acad. Sci. USA* **91**, 11733–11737 (1994).
48. Yu, J. *et al.* An integrated network of androgen receptor, polycomb, and *TMPRSS2-ERG* gene fusions in prostate cancer progression. *Cancer Cell* **17**, 443–454 (2010).
49. Issa, J.P. CpG island methylator phenotype in cancer. *Nat. Rev. Cancer* **4**, 988–993 (2004).
50. Zouridis, H. *et al.* Methylation subtypes and large-scale epigenetic alterations in gastric cancer. *Sci. Transl. Med.* **4**, 156ra140 (2012).
51. McCabe, M.T., Lee, E.K. & Vertino, P.M. A multifactorial signature of DNA sequence and polycomb binding predicts aberrant CpG island methylation. *Cancer Res.* **69**, 282–291 (2009).
52. Cho, N.Y. *et al.* Hypermethylation of CpG island loci and hypomethylation of LINE-1 and Alu repeats in prostate adenocarcinoma and their relationship to clinicopathological features. *J. Pathol.* **211**, 269–277 (2007).
53. Shyr, C.R. *et al.* Tumor suppressor PAX6 functions as androgen receptor co-repressor to inhibit prostate cancer growth. *Prostate* **70**, 190–199 (2010).
54. Nguyen, A.H. *et al.* Gata3 antagonizes cancer progression in *Pten*-deficient prostates. *Hum. Mol. Genet.* **22**, 2400–2410 (2013).
55. Kypta, R.M. & Waxman, J. Wnt/β-catenin signalling in prostate cancer. *Nat. Rev. Urol.* **9**, 418–428 (2012).
56. Kashat, M. *et al.* Inactivation of AR and Notch-1 signaling by miR-34a attenuates prostate cancer aggressiveness. *Am. J. Transl. Res.* **4**, 432–442 (2012).
57. Östling, P. *et al.* Systematic analysis of microRNAs targeting the androgen receptor in prostate cancer cells. *Cancer Res.* **71**, 1956–1967 (2011).
58. Shi, X.B. *et al.* Tumor suppressive miR-124 targets androgen receptor and inhibits proliferation of prostate cancer cells. *Oncogene* **32**, 4130–4138 (2013).
59. Dawson, M.A., Kouzarides, T. & Huntly, B.J. Targeting epigenetic readers in cancer. *N. Engl. J. Med.* **367**, 647–657 (2012).
60. Zhou, Y. & Grummt, I. The PHD finger/bromodomain of NoRC interacts with acetylated histone H4K16 and is sufficient for rDNA silencing. *Curr. Biol.* **15**, 1434–1438 (2005).

ONLINE METHODS

Gene expression analysis. Analysis of gene expression was performed using publically available TCGA level 3 gene expression data downloaded from the TCGA Data Portal (RNASeqV2 data). Analysis was restricted to patients with matched tumor and normal samples. RSEM ratio values (RSEM(tumor)/RSEM(matched normal)) were used to quantify mRNA expression levels[61]. Statistical evaluation was performed by paired *t* test. Expression data from Brase *et al.* were downloaded from the GEO database (GSE54516). Genes showing altered expression (FDR $q < 0.05$; displayed in **Supplementary Table 1**) were ranked according to the degree of expression difference in each data set. Data used for the measurement of *BAZ2A* and *EZH2* expression in metastatic samples were downloaded from the GEO database (GSE3325 and GSE6919). For the investigation of potential mechanisms of BAZ2A downregulation, data from 12 prostate cancer samples were obtained from the European Genome-phenome Archive (hosted at the European Bioinformatics Institute; accession EGAS00001000400), which includes whole-genome sequencing, mate-pair genome sequencing, methylcytosine immunoprecipitation (MCIp) sequencing, RNA sequencing and miRNA sequencing data[2]. MiRNA targeting prediction was performed using miRGator[22]. Low-abundance miRNAs were filtered out by including only miRNAs with a coverage of at least 1,000 reads in normal and prostate cancer samples. Validation of miR-133a expression was performed on samples from Brase *et al.* using quantitative PCR. Statistical significance was evaluated by *t* test.

Cell culture. All the indicated cell lines were purchased from the American Type Culture Collection. PC3 cells were cultured in RPMI 1640 medium and Ham's F12 medium (1:1; Gibco) containing 10% FBS (Gibco) and 1% penicillin-streptomycin (Gibco). RWPE1 cells were cultured in Keratinocyte-SFM medium (Gibco) supplemented with human recombinant epidermal growth factor 1-53 (EGF 1-53) and bovine pituitary extract (BPE) and 1% penicillin-streptomycin. DU 145, LNCaP and BPH1 cells were cultured in RPMI 1640 medium containing 10% FBS and 1% penicillin-streptomycin. All cells were regularly tested for mycoplasma contamination.

Evaluation of miRNA targeting. Luciferase assays were performed in HEK293T cells grown in DMEM. Cells grown in 384-well plates were transfected with 5 nM miRNA mimics (Qiagen) or non-targeting control (AllStar Negative Control, Qiagen) using DharmaFECT1 (Thermo Fisher Scientific). *BAZ2A* 3′ UTR fragments of 300–1,609 bp in length were cloned into the pMIR-Report vector (Ambion) 3′ to the firefly luciferase gene. The predicted miR-133a binding site was mutated using the QuikChange Site-Directed Mutagenesis kit (Stratagene). After 24 h, 0.3 ng of each pMIR-Report-BAZ2A 3′ UTR construct was mixed with 10 ng of the TK-*Renilla* plasmid (Promega) and was transfected into cells using TransIT-LT1 transfection reagent (Mirus Bio) with six replicates per construct. The readout was assessed 48 h after reporter transfection, as previously described[62]. Firefly luciferase activity was normalized to *Renilla* luciferase activity, and the average of technical replicates was calculated. Each experiment was performed in triplicate.

siRNA and shRNA transfections. Cells were seeded at a density of 12,000 cells/cm^2 and transfected with the indicated siRNAs using Lipofectamine RNAiMAX (Invitrogen) in Opti-MEM I Reduced-Serum Medium (Gibco). To achieve high siRNA transfection efficiencies, we performed reverse transfection in PC3 and DU145 cells and forward transfection in RWPE1 and LNCaP cells. Knockdown was analyzed 3–4 d after transfection by qRT-PCR or protein blot. Sequences encoding control shRNA and shRNA to *BAZ2A* were cloned into lentiviral vectors. Lentiviruses were generated in HEK293 cells and used to transduce 1×10^6 PC3 cells seeded on a 10-cm dish. Stable clones were selected with puromycin (0.4 µg/ml; Gibco).

RNA isolation, reverse transcription and quantitative RT-PCR. RNA was purified with TRIzol reagent (Invitrogen) according to the manufacturer's protocol. RNA (1 µg) was reverse transcribed using random hexamers. qRT-PCR was performed on a Rotor-Gene RG-3000 A (Corbett Research) using the SensiMix SYBR Hi-ROX Mix (Bioline). Relative transcription levels were determined by normalizing to *GAPDH* or *ACTB* mRNA levels. The statistical significance (*P* value) of the difference in expression levels for a gene was calculated using a two-sample paired *t* test. Sequences for the primer used in qRT-PCR are listed in **Supplementary Table 12**.

Cell proliferation assays. Twenty-four hours after transfection with the relevant siRNA or miRNA, cells (1×10^5) were seeded in 6-well plates. On each following day, cells from two distinct wells were counted using a cell counter (CASY, model TT, Roche). For WST1 assays, 1 d after siRNA transfections, 3×10^3 (PC3) or 4×10^3 (RWPE1) cells were seeded in each well of a 96-well plate. Cell proliferation and viability were determined every following day by the addition of Cell Proliferation Reagent WST-1 (Roche) according to the manufacturer's instructions.

Immunofluorescence. Cells were grown on coverslips coated with 0.01% poly-L-lysine (Sigma-Aldrich) and permeabilized with 0.05% Triton X-100 in 20 mM Tris-HCl (pH 8), 5 mM $MgCl_2$, 0.5 mM EDTA and 25% glycerol. After washing with PBS, cells were fixed with cold methanol (7 min) and stained with antibodies to BAZ2A (Diagenode, CS-090-100; 1:40 dilution) and UBF (Santa Cruz Biotechnology, sc-13125; 1:40 dilution) and with Hoechst 33258 (Sigma-Aldrich). Immunofluorescent images were digitally recorded with a Leica DMI 6000 B microscope.

Cell synchronization and FACS analysis. Cells were synchronized at G1/S through treatment with 2 mM thymidine (Sigma-Aldrich) for 14 h, released for 9 h and then treated for 14 h with 400 µM L-mimosine (Sigma-Aldrich). After being released from the L-mimosine block (here referred to as $t = 0$ h), cells at the indicated time points were trypsinized, washed with PBS, fixed with ice-cold ethanol at −20 °C and stained with propidium iodide (20 µg/ml). Cell cycle analysis was performed by flow cytometry on a CyAn ADP Analyzer (Beckman Coulter).

Colony formation assays. Cells were seeded in 6-well plates at a concentration of 500 cells/well and grown for 8 d. The colony formation potential of each clone expressing control shRNA or shRNA to *BAZ2A* was determined in triplicate using three six-well plates. Cells were stained with crystal violet (0.5% crystal violet in 20% methanol) for 3 min, destained by washing three times with 2 ml of water and air dried.

Boyden chamber invasion assays. Twenty-four hours after transfection, cells were starved for 24 h in growth medium containing 1% FBS. Boyden chamber invasion assays were performed according to the manufacturer's protocol. Briefly, 40,000 cells were subjected to Matrigel-coated cell inserts (BD Biosciences, 354480) in starvation medium (0% FBS). Growth medium containing 10% FBS was used as a chemoattractant for 18 h. Invaded cells were fixed with 100% methanol and visualized using Hoechst 33258 (Sigma-Aldrich). Membranes were mounted to glass slides, and cell numbers were quantified using a DMI6000 B microscope (Leica).

Scratch wound healing assays. siRNA-treated PC3 cells were seeded in triplicate in six-well plates and grown until confluent. Identical scratches were generated with a 1,000-µl plastic pipette tip. Any cellular debris was removed by medium replacement. After 24 h, closure of the scratch by migrating cells was analyzed with an Olympus CKX31 microscope.

Senescence and apoptosis assays. Cellular senescence was analyzed with the Senescence β-Galactosidase Staining kit (Cell Signaling) according to the manufacturer's protocol. Apoptosis was investigated using the FITC Annexin V Apoptosis Detection Kit I (BD Biosciences) following the manufacturer's instructions, and subsequent FACS analysis was performed on a CyAn ADP Analyzer (Beckman Coulter).

PC3 and RWPE1 gene expression microarrays. Three (PC3 cells) or two (RWPE1 cells) independent knockdown experiments were performed for gene expression microarray analysis. RNA was isolated using the NucleoSpin RNA II kit (Macherey-Nagel) followed by on-column DNase digestion to remove any contaminating genomic DNA. Total RNA (100 ng) was reverse transcribed to double-stranded cDNA, which was linearly amplified and labeled with Cy3. After quantification using the NanoDrop spectrophotometer (Witec) and quality

assessment with the Agilent 2100 Bioanalyzer (Agilent Technologies), 1.6 µg of Cy3-labeled cRNA was hybridized to SurePrint G3 Human Exon 4x180K microarrays (Agilent Technologies) according to the manufacturer's protocol. Arrays were scanned with an Agilent G2565CA Microarray Scanner System (Scan Control Software 8.5, Agilent Technologies). Raw intensity data were obtained using Agilent's Feature Extraction Software version 10.7 for array image analysis and the calculation of spot intensity measurements. Data were analyzed with R Bioconductor. Between-array normalization was performed using quantile normalization. Differential expression was computed using the limma package. Heat maps were generated using the heatmap.2 function in the gplots package. Transcripts with a fold change of >1.5 or <0.66 ($\log_2 \pm 0.58$) in cells expressing *BAZ2A* or *EZH2* siRNA relative to control cells and $P < 0.05$ were considered to have a statistically significant difference in expression and were analyzed for GO enrichment using the Database for Annotation, Visualization and Integrated Discovery (DAVID) for the enrichment of GO terms.

Immunoprecipitation. Immunoprecipitation was performed by transfection of HEK293T cells with the expression vector pcDNA-Flag-HA-BAZ2A. Nuclear extracts were immunoprecipitated overnight at 4 °C using an immobilized antibody against Flag (Anti-FLAG M2 Affinity Gel, Sigma). Precipitates were washed three times with wash buffer (20 mM Tris-HCl (pH 7.8), 150 mM KCl, 5 mM $MgCl_2$, 0.2 mM EDTA, 10% glycerol, 0.1% Tween and 0.1 mM PMSF), separated on a 6% SDS-polyacrylamide gel and analyzed by immunoblotting.

Chromatin immunoprecipitation. ChIP analysis was performed as previously described[63]. Briefly, 1% formaldehyde was added to cultured cells to cross-link proteins to DNA. Isolated nuclei were then lysed in 300 µl of lysis buffer (50 mM Tris-HCl (pH 8.1), 10 mM EDTA and 1% SDS) and sonicated using a Bioruptor ultrasonic cell disruptor (Diagenode) to shear genomic DNA to an average fragment size of 200 bp. Chromatin (20 µg) was diluted tenfold with immunoprecipitation buffer (16.7 mM Tris-HCl (pH 8.1), 167 mM NaCl, 1.2 mM EDTA, 0.01% SDS and 1.1% Triton X-100) and then immunoprecipitated overnight with the indicated antibodies. After washing, elution and reversion of cross-links, the precipitated DNA was purified with phenol-chloroform, ethanol precipitated and quantified by quantitative PCR. Primer sequences and antibodies are listed in **Supplementary Tables 12** and **13**.

DNA methylation data analysis. Prostate tumor samples were selected histologically to have >70% tumor content. DNA was isolated from formalin-fixed paraffin-embedded material using the QIAamp DNA FFPE Tissue kit (Qiagen). DNA methylation analysis was performed using 450K BeadChip arrays (Illumina) according to the manufacturer's instructions. We extracted the raw methylation intensity data and performed subset quantile within-array normalization (SWAN)[46]. Probes with a detection *P* value of <0.01 were excluded from further analysis. The 5,000 most variable probes were selected for *k*-means consensus clustering by the ConsensusClusterPlus package with Spearman distance and average linkage over 1,000 resampling iterations with random restart. The optimal number of clusters was determined by the CDF and consensus clustering. Hierarchical clustering was then performed to visualize the methylation patterns within 35 samples. Gene set enrichment analysis was performed using GSEA tools (version 2-2.0.13) with Molecular Signatures Databases (MSigDB version 4.0) from the Broad Institute as previous described[64] with modifications. Statistical enrichment of the intersection of the gene lists for differential methylation and expression was performed using random permutation.

Tissue microarrays. Radical prostatectomy specimens were obtained from 11,152 patients undergoing surgery between 1992 and 2011 at the Department of Urology and the Martini Clinics at the University Medical Center Hamburg-Eppendorf. Follow-up data were available for a total of 9,628 patients, with a median follow-up of 36.8 months (range of 1 to 228 months; **Supplementary Table 9**). PSA values were measured quarterly during the first 3 years and then biannually following surgery, and recurrence was defined as a postoperative PSA value of 0.2 ng/ml and increasing at first appearance. All prostate specimens were analyzed according to a standard procedure, including complete embedding of the entire prostate for histological analysis[65]. The TMA manufacturing process was described earlier in detail[66]. All histological sections stained with hematoxylin and eosin from all prostatectomy specimens were reviewed for the purpose of this study, and the positions of tumors were marked on the slides. One 0.6-mm tissue core was punched from a preselected area of each tumor and transferred in a TMA. The punch site was selected to contain the highest possible fraction of tumor cells. The tissues were distributed among 24 TMA blocks, each containing 144 to 522 tumor samples. Presence or absence of cancer tissue was validated by immunohistochemical AMACR and 34BE12 analysis on adjacent TMA sections. For internal controls, each TMA block also contained various control tissues, including normal prostate tissue.

Immunohistochemistry. Freshly cut TMA sections were immunostained in a single day and as one experiment. Primary antibody specific for BAZ2A (polyclonal, rabbit, Abnova, PAB21919; 1:150 dilution) was applied, and slides were deparaffinized and exposed to heat-induced antigen retrieval for 5 min in an autoclave at 121 °C in pH 7.8 Tris-EDTA buffer. Bound antibody was visualized using the EnVision kit (Dako). All stainings were analyzed by a single, experienced individual (K.G.). BAZ2A expression was predominantly localized to the nucleus, with lower expression levels in the cytoplasm of the cells. Nuclear BAZ2A staining was evaluated according to the following scoring system. The staining intensity (0, 1+, 2+ and 3+) and fraction of positive tumor cells were recorded for each tissue spot. A final immunohistochemistry score was built from these parameters as previously described[67–69]. Negative scores indicated the complete absence of staining; weak scores indicated a staining intensity of 1+ in ≤70% of tumor cells or a staining intensity of 2+ in ≤30% of tumor cells; moderate scores indicated a staining intensity of 1+ in >70% of tumor cells, a staining intensity of 2+ in >30% but ≤70% of tumor cells or a staining intensity of 3+ in ≤30% of tumor cells; and strong scores indicated a staining intensity of 2+ in >70% of tumor cells or a staining intensity of 3+ in >30% of tumor cells. As cytoplasmic BAZ2A staining was rare and typically associated with high nuclear staining levels, it was thus not considered for analysis.

Statistical analysis. To calculate whether the proportion of genes regulated by both BAZ2A and EZH2 was expected by chance, we used a combination of permutation and Fisher tests to calculate *P* values. Briefly, the number of overlaps between BAZ2A- and EZH2-regulated genes was determined, and we then performed random permutation of EZH2-regulated genes and computed the overlap with BAZ2A-regulated genes using 1,000 iterations. From the permutation, the mean numbers of overlapped and non-overlapped genes were obtained. Fisher's exact test was used to evaluate the statistical difference from the expected pattern.

Multivariate analysis. Four multivariate analyses were performed evaluating the clinical relevance of BAZ2A expression in different scenarios (listed in **Supplementary Table 9**). Scenario 1 used all postoperatively available parameters, including clinical stage, nodal status, margin status, preoperative PSA value and Gleason grade obtained on the resected prostate. Scenario 2 used all postoperatively available parameters with the exception of nodal status. The rationale for this approach was that lymphadenectomy is not a routine procedure in the surgical therapy of prostate cancer and that excluding nodal status in multivariate analysis increases case number. The next two scenarios tried to better model the preoperative situation. Scenario 3 included BAZ2A expression, preoperative PSA value, clinical stage and the Gleason grade obtained on the prostatectomy specimen. Because postoperative Gleason grade varies from preoperative Gleason grade, another multivariate analysis was added as scenario 4. In this scenario, the preoperative Gleason grade obtained on the original diagnostic biopsy was combined with the preoperative PSA value, clinical stage and BAZ2A expression.

61. Li, B. & Dewey, C.N. RSEM: accurate transcript quantification from RNA-Seq data with or without a reference genome. *BMC Bioinformatics* **12**, 323 (2011).
62. Metzig, M. *et al.* An RNAi screen identifies USP2 as a factor required for TNF-α–induced NF-κB signaling. *Int. J. Cancer* **129**, 607–618 (2011).
63. Santoro, R. Analysis of chromatin composition of repetitive sequences: the ChIP-Chop assay. *Methods Mol. Biol.* **1094**, 319–328 (2014).
64. Subramanian, A., Kuehn, H., Gould, J., Tamayo, P. & Mesirov, J.P. GSEA-P: a desktop application for Gene Set Enrichment Analysis. *Bioinformatics* **23**, 3251–3253 (2007).

doi:10.1038/ng.3165

65. Schlomm, T. *et al*. Clinical significance of p53 alterations in surgically treated prostate cancers. *Mod. Pathol.* **21**, 1371–1378 (2008).
66. Mirlacher, M. & Simon, R. Recipient block TMA technique. *Methods Mol. Biol.* **664**, 37–44 (2010).
67. Minner, S. *et al*. High level PSMA expression is associated with early PSA recurrence in surgically treated prostate cancer. *Prostate* **71**, 281–288 (2011).
68. Grupp, K. *et al*. Cysteine-rich secretory protein 3 overexpression is linked to a subset of *PTEN*-deleted *ERG* fusion–positive prostate cancers with early biochemical recurrence. *Mod. Pathol.* **26**, 733–742 (2013).
69. Muller, J. *et al*. Loss of pSer2448-mTOR expression is linked to adverse prognosis and tumor progression in *ERG*-fusion-positive cancers. *Int. J. Cancer* **132**, 1333–1340 (2013).